General synthesis of complex analogue filters

C. Cuypers, N.Y. Voo, M. Teplechuk and J.I. Sewell

Abstract: General methods for the synthesis of complex band-pass and band-stop analogue filters are developed for implementation by active-RC, gm-C, switched-capacitor (SC) and switched-current (SI) techniques. These principles are extended to synthesis procedures for log-domain complex realisations. Circuits for filters and group delay equalisers are presented for both ladder and cascade-biquad realisations. These have been incorporated into the filter design software XFILTER. Various designs are compared, noise and sensitivity responses being shown.

1 Introduction

Complex (polyphase) filters are finding many applications today [1–7], especially in the communications area. They are essentially integrated circuit filters and, in order to cover the different frequency ranges of application, it is necessary to encompass different implementation techniques, such as active-RC, gm-C, switched-capacitor (SC), switched-current (SI) and log-domain. It is also important to develop a general synthesis method without undue restrictions on order and filter characteristic.

A complex band-pass transfer function $H_C(s)$ is derived from a low-pass transfer function $H(s)$ by the frequency shift method using the substitution $(s \rightarrow s - j\omega_{sh})$ giving $H_C(s) = H(s - j\omega_{sh})$, where ω_{sh} is the shift frequency. In general the coefficients of $H_C(s)$ are complex [5], therefore $H_C(s)$ can be represented as $H_C(s) = H^{\mathrm{Re}}(s) + jH^{\mathrm{Im}}(s)$, where both real $H^{\mathrm{Re}}(s)$ and imaginary $H^{\mathrm{Im}}(s)$ parts are real transfer functions.

The input and the output signals are complex

$$X(s) = X^{\mathrm{Re}}(s) + jX^{\mathrm{Im}}(s)$$
$$Y(s) = Y^{\mathrm{Re}}(s) + jY^{\mathrm{Im}}(s)$$

The relationships between the input and output signals are

$$Y^{\mathrm{Re}}(s) = H^{\mathrm{Re}}(s)X^{\mathrm{Re}}(s) - H^{\mathrm{Im}}(s)X^{\mathrm{Im}}(s)$$
$$Y^{\mathrm{Im}}(s) = H^{\mathrm{Re}}(s)X^{\mathrm{Im}}(s) + H^{\mathrm{Im}}(s)X^{\mathrm{Re}}(s)$$

and represented in Fig. 1.

The frequency shift method, which leads to two identical low-pass filters connected by a cross-coupling network, has been used successfully [6, 7]. This is now formalised for ladder-derived filters in all the above realisation techniques. Extension to the design of band-stop filters follows easily and essentially comprises two identical high-pass networks with cross-coupling elements. Cascade biquad designs are also produced and have some value as practical realisations, mainly because of their simplicity. Equalisation of group delay in these complex realisations is often required and the techniques have been extended to include this with both ladder and biquad implementations. General implementation of all these procedures in the XFILTER software is available and provides a useful design tool. Comparison of designs is shown in numerous examples.

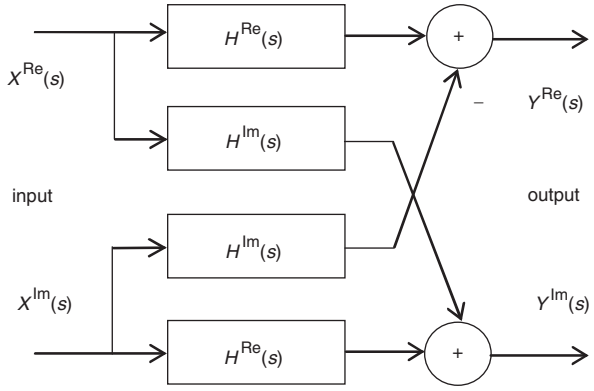

Fig. 1 *Schematic representation of a complex analogue filter*

2 Ladder-derived continuous-time complex band-pass filters

The nodal equation of a passive ladder is described by

$$(s\boldsymbol{C} + s^{-1}\boldsymbol{\Gamma} + \boldsymbol{G})\boldsymbol{V} = \boldsymbol{J} \qquad (1)$$

where $\boldsymbol{C}$, $\boldsymbol{\Gamma}$ and $\boldsymbol{G}$ are admittance matrices of capacitors, inverse inductors and resistors, respectively. $\boldsymbol{V}$ and $\boldsymbol{J}$ are vectors representing the nodal voltages and input current sources. The system is decomposed into two related first-order systems, which can be implemented, directly by active-RC or gm-C circuits. The decomposition [8] is performed on the left matrix $\boldsymbol{C}$ or the right matrix $\boldsymbol{\Gamma}$.

For a left matrix decomposition $\boldsymbol{C} = \boldsymbol{C}_l\boldsymbol{C}_r$ then

$$\boldsymbol{C}_l\boldsymbol{W} = -\frac{1}{s}\boldsymbol{G}\boldsymbol{V} - \boldsymbol{G}\boldsymbol{V} - (-\boldsymbol{J})$$
$$\boldsymbol{C}_r\boldsymbol{V} = \frac{1}{s}\boldsymbol{W}$$

For a right matrix decomposition $\boldsymbol{\Gamma} = \boldsymbol{\Gamma}_l\boldsymbol{\Gamma}_r$ then

$$\boldsymbol{C}_l\boldsymbol{V} = -\frac{1}{s}(\boldsymbol{\Gamma}_l\boldsymbol{W} + \boldsymbol{G}\boldsymbol{V} - \boldsymbol{J})$$
$$\boldsymbol{I}_D\boldsymbol{W} = \frac{1}{s}\boldsymbol{\Gamma}_r\boldsymbol{V}$$

IEE Proceedings online no. 20040816

doi:10.1049/ip-cds:20040816

Paper first received 14th July 2003 and in revised form 11th May 2004

C. Cuypers, M. Teplechuk and J.I. Sewell are with the Department of Electronics and Electrical Engineering, University of Glasgow, Glasgow G12 8LT, UK

N.Y. Voo is with the Department of Electronics and Computer Science, University of Southampton, Southampton SO17 1BJ, UK

where $\boldsymbol{W}$ is an auxiliary vector of intermediate variables and $\boldsymbol{I}_D$ is the identity matrix.

Using the frequency shift transformation ($s \rightarrow s - j\omega_{sh}$), the left matrix decomposition becomes

$$\begin{aligned}\boldsymbol{C}_l\boldsymbol{W} = &-\frac{1}{s}(\boldsymbol{\Gamma}\boldsymbol{V} - j\omega_{sh}\boldsymbol{C}_l\boldsymbol{W} \\ &- j\omega_{sh}\boldsymbol{G}\boldsymbol{V} + j\omega_{sh}\boldsymbol{J}) - \boldsymbol{G}\boldsymbol{V} + \boldsymbol{J} \\ \boldsymbol{C}_r\boldsymbol{V} = &\frac{1}{s}(\boldsymbol{W} + j\omega_{sh}\boldsymbol{C}_r\boldsymbol{V})\end{aligned}$$

and the right matrix decomposition

$$\begin{aligned}\boldsymbol{C}\boldsymbol{V} = &\frac{-1}{s}(\boldsymbol{\Gamma}_l\boldsymbol{W} + \boldsymbol{G}\boldsymbol{V} - \boldsymbol{J} - j\omega_{sh}\boldsymbol{C}\boldsymbol{V}) \\ \boldsymbol{I}_D\boldsymbol{W} = &\frac{1}{s}(\boldsymbol{\Gamma}_r\boldsymbol{V} + j\omega_{sh}\boldsymbol{W})\end{aligned}$$

The complex transfer functions are available from two sets of equations.

Left matrix decompositions

For real transfer functions:

$$\begin{aligned}\boldsymbol{C}_l\boldsymbol{W}^{\mathrm{Re}} = &-\frac{1}{s}(\boldsymbol{\Gamma}\boldsymbol{V}^{\mathrm{Re}} + \omega_{sh}\boldsymbol{C}_l\boldsymbol{W}^{\mathrm{Im}} \\ &+ \omega_{sh}\boldsymbol{G}\boldsymbol{V}^{\mathrm{Im}} - \omega_{sh}\boldsymbol{J}^{\mathrm{Im}}) - \boldsymbol{G}\boldsymbol{V}^{\mathrm{Re}} + \boldsymbol{J}^{\mathrm{Re}} \\ \boldsymbol{C}_r\boldsymbol{V}^{\mathrm{Re}} = &\frac{1}{s}(\boldsymbol{W}^{\mathrm{Re}} - \omega_{sh}\boldsymbol{C}_r\boldsymbol{V}^{\mathrm{Im}})\end{aligned}$$

For imaginary transfer functions

$$\begin{aligned}\boldsymbol{C}_l\boldsymbol{W}^{\mathrm{Im}} = &-\frac{1}{s}(\boldsymbol{\Gamma}\boldsymbol{V}^{\mathrm{Im}} - \omega_{sh}\boldsymbol{C}_l\boldsymbol{W}^{\mathrm{Re}} \\ &- \omega_{sh}\boldsymbol{G}\boldsymbol{V}^{\mathrm{Re}} + \omega_{sh}\boldsymbol{J}^{\mathrm{Re}}) - \boldsymbol{G}\boldsymbol{V}^{\mathrm{Im}} + \boldsymbol{J}^{\mathrm{Im}} \\ \boldsymbol{C}_r\boldsymbol{V}^{\mathrm{Im}} = &\frac{1}{s}(\boldsymbol{W}^{\mathrm{Im}} - \omega_{sh}\boldsymbol{C}_r\boldsymbol{V}^{\mathrm{Re}})\end{aligned}$$

Right matrix decompositions

For real transfer functions:

$$\begin{aligned}\boldsymbol{C}\boldsymbol{V}^{\mathrm{Re}} = &-\frac{1}{s}(\boldsymbol{\Gamma}_l\boldsymbol{W}^{\mathrm{Re}} + \boldsymbol{G}\boldsymbol{V}^{\mathrm{Re}} - \boldsymbol{J}^{\mathrm{Re}} + \omega_{sh}\boldsymbol{C}\boldsymbol{V}^{\mathrm{Im}}) \\ \boldsymbol{I}_D\boldsymbol{W}^{\mathrm{Re}} = &\frac{1}{s}(\boldsymbol{\Gamma}_r\boldsymbol{V}^{\mathrm{Re}} - \omega_{sh}\boldsymbol{W}^{\mathrm{Im}})\end{aligned}$$

For imaginary transfer functions:

$$\begin{aligned}\boldsymbol{C}\boldsymbol{V}^{\mathrm{Im}} = &-\frac{1}{s}(\boldsymbol{\Gamma}_l\boldsymbol{W}^{\mathrm{Im}} + \boldsymbol{G}\boldsymbol{V}^{\mathrm{Im}} - \boldsymbol{J}^{\mathrm{Im}} - \omega_{sh}\boldsymbol{C}\boldsymbol{V}^{\mathrm{Re}}) \\ \boldsymbol{I}_D\boldsymbol{W}^{\mathrm{Im}} = &\frac{1}{s}(\boldsymbol{\Gamma}_r\boldsymbol{V}^{\mathrm{Im}} - \omega_{sh}\boldsymbol{W}^{\mathrm{Re}})\end{aligned}$$

The complex band-pass filter realisation therefore consists of two identical real low-pass filters cross-coupled via resistances (terms in ω_{sh}). A range of active-RC implementations is available from a number of decompositions [8].

A number of gm-C ladder decompositions are aimed at producing equal transconductance values, one of these, the TC topological decomposition [9], is used to produce a complex band-pass filter. With $\boldsymbol{\Gamma} = \boldsymbol{A}\boldsymbol{D}\boldsymbol{A}^T$, where $\boldsymbol{D}$ is a diagonal matrix of inverse inductance values and $\boldsymbol{A}$ is an incidence matrix, the following pair of equations is equivalent to (1), (g is a scaling conductance and $\boldsymbol{C}_L = g^2\boldsymbol{D}^{-1}$):

$$\begin{aligned}\boldsymbol{C}\boldsymbol{V} = &\frac{1}{s}(\boldsymbol{J} - \boldsymbol{G}\boldsymbol{V} - g\boldsymbol{A}\boldsymbol{W}) \\ \boldsymbol{C}_L\boldsymbol{W} = &\frac{1}{s}(g\boldsymbol{A}^T\boldsymbol{V})\end{aligned}$$

Applying the shift frequency transformation gives

$$\begin{aligned}\boldsymbol{C}\boldsymbol{V} = &\frac{1}{s}(\boldsymbol{J} - \boldsymbol{G}\boldsymbol{V} - g\boldsymbol{A}\boldsymbol{W} + j\omega_{sh}\boldsymbol{C}\boldsymbol{V}) \\ \boldsymbol{C}_L\boldsymbol{W} = &\frac{1}{s}(g\boldsymbol{A}^T\boldsymbol{V} + j\omega_{sh}\boldsymbol{C}_L\boldsymbol{W})\end{aligned}$$

Which leads to gm-C complex band-pass filter implementations utilising two cross-coupled low-pass ladder realisations, though the single value of transconductance is sacrificed in the cross-coupling terms.

3 Ladder-derived sampled-data complex band-pass filters

For switched networks (SC and SI), the frequency shifting mechanism [4] is expressed as $H_C(z) = H_{lp}(ze^{-j\theta})$, where $\theta = \omega_{sh}\,T$, with ω_{sh} the shift frequency and T the sampling time. Equation (1), after bilinear transformation and some manipulation, gives

$$\left(\frac{1}{\psi}\boldsymbol{A} + \Phi\boldsymbol{B} + \boldsymbol{D}\right)\boldsymbol{V} = \boldsymbol{J}''$$

where

$$\begin{aligned}&\boldsymbol{A} = \frac{2}{T}\boldsymbol{C} + \frac{T}{2}\boldsymbol{\Gamma} + \boldsymbol{G},\ \boldsymbol{B} = 2T\boldsymbol{\Gamma},\ \boldsymbol{D} = 2\boldsymbol{G} \text{ and} \\ &\boldsymbol{J}'' = (1+z)\boldsymbol{J}. \\ &\Psi = \frac{z^{-1}}{1-z^{-1}} \text{ and } \Phi = \frac{1}{1-z^{-1}}\end{aligned}$$

represent forward and backward Euler integrators, respectively [8].

A left matrix decomposition is

$$\begin{aligned}\boldsymbol{A}_l\boldsymbol{W} = &-(\Phi\boldsymbol{B} + \boldsymbol{D})\boldsymbol{V} - 2(-\boldsymbol{J}) \\ \boldsymbol{A}_r\boldsymbol{V} = &\boldsymbol{\Psi}\boldsymbol{W} - \boldsymbol{A}_l^{-1}(-\boldsymbol{J})\end{aligned}$$

In general $\boldsymbol{A} = \boldsymbol{L}\boldsymbol{U}$, $\boldsymbol{A} = \boldsymbol{U}\boldsymbol{L}$, $\boldsymbol{A} = \boldsymbol{I}\boldsymbol{A}$, $\boldsymbol{A} = \boldsymbol{A}\boldsymbol{I}$ are the various decompositions.

Substituting LDI integrator operators into the above equations

$$\begin{aligned}\boldsymbol{A}_l\boldsymbol{W} = &-\frac{1}{1-z^{-1}}\boldsymbol{B}\boldsymbol{V} - \boldsymbol{D}\boldsymbol{V} - 2(-\boldsymbol{J}) \\ \boldsymbol{A}_r\boldsymbol{V} = &\frac{z^{-1}}{1-z^{-1}}\boldsymbol{W} - A_l^{-1}(-\boldsymbol{J})\end{aligned}$$

Applying a frequency shift ($z \rightarrow ze^{-j\theta}$) to obtain the complex transfer functions gives

$$\begin{aligned}\boldsymbol{A}_l\boldsymbol{W} = &\boldsymbol{A}_l\boldsymbol{W}z^{-1}e^{j\theta} - \boldsymbol{B}\boldsymbol{V} - \boldsymbol{D}\boldsymbol{V} \\ &+ \boldsymbol{D}\boldsymbol{V}z^{-1}e^{j\theta} - 2(-\boldsymbol{J}) + 2(-\boldsymbol{J})z^{-1}e^{j\theta} \\ \boldsymbol{A}_r\boldsymbol{V} = &\boldsymbol{A}_r\boldsymbol{V}z^{-1}e^{j\theta} + \boldsymbol{W}z^{-1}e^{j\theta} - \boldsymbol{A}_l^{-1}(-\boldsymbol{J}) \\ &+ \boldsymbol{A}_l^{-1}(-\boldsymbol{J})\boldsymbol{z}^{-1}\boldsymbol{e}^{j\theta}\end{aligned}$$

Substituting $e^{j\theta} = \cos\theta + j\sin\theta$ will lead to two low-pass filters with cross-coupling and modified internal topologies, which increase the complexity of circuit design. However, for a sufficiently high clock rate ($\omega_{clk}/\omega_{sh} > 40$), $\cos\theta \cong 1$ then

$$\begin{aligned}\boldsymbol{A}_l\boldsymbol{W} = &(\Phi\boldsymbol{B} - \boldsymbol{D})\boldsymbol{V} - 2(-\boldsymbol{J}) + j\,2(-\boldsymbol{J})\Psi\,\sin\theta \\ &+ j\boldsymbol{A}_l\boldsymbol{W}\Psi\,\sin\theta + j\boldsymbol{D}\boldsymbol{V}\Psi\,\sin\theta \\ \boldsymbol{A}_r\boldsymbol{V} = &\boldsymbol{W}\Psi - \boldsymbol{A}_l^{-1}(-\boldsymbol{J}) + j\boldsymbol{A}_l^{-1}(-\boldsymbol{J})\Psi\,\sin\theta \\ &+ j\boldsymbol{A}_r\boldsymbol{V}\Psi\,\sin\theta + j\boldsymbol{W}\Psi\,\sin\theta\end{aligned}$$

Complex transfer functions are described by two sets of equations:

For real transfer functions

$$\boldsymbol{A}_l\boldsymbol{W}^{\mathrm{Re}} = -(\Phi\boldsymbol{B} - \boldsymbol{D}(1-z^{-1}))\boldsymbol{V}^{\mathrm{Re}} - 2(-\boldsymbol{J}) - 2(-\boldsymbol{J}^{\mathrm{Im}})\Phi\sin\theta - \boldsymbol{A}_l\boldsymbol{W}^{\mathrm{Im}}\Phi\sin\theta - \boldsymbol{D}\boldsymbol{V}^{\mathrm{Im}}\Phi\sin\theta$$

$$\boldsymbol{A}_r\boldsymbol{V}^{\mathrm{Re}} = \boldsymbol{W}^{\mathrm{Re}}\Psi - \boldsymbol{A}_l^{-1}(-\boldsymbol{J}^{\mathrm{Re}}) - \boldsymbol{A}_l^{-1}(-\boldsymbol{J}^{\mathrm{Im}})\Phi\sin\theta - \boldsymbol{A}_r\boldsymbol{V}^{\mathrm{Im}}\Phi\sin\theta - \boldsymbol{W}^{\mathrm{Im}}\Phi\sin\theta$$

For imaginary transfer functions:

$$\boldsymbol{A}_l\boldsymbol{W}^{\mathrm{Im}} = -(\Phi\boldsymbol{B} - \boldsymbol{D}(1-z^{-1}))\boldsymbol{V}^{\mathrm{Im}} - 2(-\boldsymbol{J}) + 2(-\boldsymbol{J}^{\mathrm{Re}})\Psi\sin\theta + \boldsymbol{A}_l\boldsymbol{W}^{\mathrm{Re}}\Psi\sin\theta + \boldsymbol{D}\boldsymbol{V}^{\mathrm{Re}}\Psi\sin\theta$$

$$\boldsymbol{A}_r\boldsymbol{V}^{\mathrm{Im}} = \boldsymbol{W}^{\mathrm{Im}}\Psi - \boldsymbol{A}_l^{-1}(-\boldsymbol{J}^{\mathrm{Im}}) + \boldsymbol{A}_l^{-1}(-\boldsymbol{J}^{\mathrm{Re}})\Psi\sin\theta + \boldsymbol{A}_r\boldsymbol{V}^{\mathrm{Re}}\Psi\sin\theta\Psi + \boldsymbol{W}^{\mathrm{Re}}\Psi\sin\theta$$

Now a complex SC band-pass circuit can be obtained from two identical low-pass circuits with cross-couplings.

A right matrix decomposition is

$$\boldsymbol{A}\boldsymbol{V} = -\Phi(\boldsymbol{B}_l\boldsymbol{W} + \boldsymbol{D}\boldsymbol{V}) + \boldsymbol{J}$$

$$\boldsymbol{W} = \Psi\boldsymbol{B}_r\boldsymbol{V} - 2\boldsymbol{B}_l^{-1}\boldsymbol{J}$$

where $\boldsymbol{B}_l$ and $\boldsymbol{B}_r$ are the factors of the right-hand matrix $\boldsymbol{B}$. In general $\boldsymbol{B}$ is decomposed as $\boldsymbol{LU}$, $\boldsymbol{UL}$, $\boldsymbol{IA}$ and $\boldsymbol{AI}$.

Applying the frequency-shift transformation and some manipulation gives two sets of equations, which yield the complex transfer functions.

For real transfer functions:

$$\boldsymbol{A}\boldsymbol{V}^{\mathrm{Re}} = -\Phi(\boldsymbol{B}_l\boldsymbol{W}^{\mathrm{Re}} + \boldsymbol{D}\boldsymbol{V}^{\mathrm{Re}}) + \boldsymbol{J}^{\mathrm{Re}} - \boldsymbol{J}^{\mathrm{Im}}\Phi\sin\theta - \boldsymbol{A}\boldsymbol{V}^{\mathrm{Im}}\Phi\sin\theta$$

$$\boldsymbol{W}^{\mathrm{Re}} = \boldsymbol{B}_r\boldsymbol{V}^{\mathrm{Re}}\Psi - 2\boldsymbol{B}_l^{-1}\boldsymbol{J}^{\mathrm{Re}} - 2\boldsymbol{B}_l^{-1}\boldsymbol{J}^{\mathrm{Im}}\Phi\sin\theta - \boldsymbol{B}_r\boldsymbol{V}^{\mathrm{Im}}\Phi\sin\theta - \boldsymbol{W}^{\mathrm{Im}}\Phi\sin\theta$$

For imaginary transfer functions

$$\boldsymbol{A}\boldsymbol{V}^{\mathrm{Im}} = -\Phi(\boldsymbol{B}_l\boldsymbol{W}^{\mathrm{Im}} + \boldsymbol{D}\boldsymbol{V}^{\mathrm{Im}}) + \boldsymbol{J}^{\mathrm{Im}} + \boldsymbol{J}^{\mathrm{Re}}\Psi\sin\theta + \boldsymbol{A}\boldsymbol{V}^{\mathrm{Re}}\Psi\sin\theta$$

$$\boldsymbol{W}^{\mathrm{Im}} = \boldsymbol{B}_r\boldsymbol{V}^{\mathrm{Im}}\Psi - 2\boldsymbol{B}_l^{-1}\boldsymbol{J}^{\mathrm{Im}} + 2\boldsymbol{B}_l^{-1}\boldsymbol{J}^{\mathrm{Re}}\Psi\sin\theta + \boldsymbol{B}_r\boldsymbol{V}^{\mathrm{Re}}\Psi\sin\theta + \boldsymbol{W}^{\mathrm{Re}}\Psi\sin\theta$$

Which again yield complex SC band-pass realisations utilising two cross-coupled low-pass circuits.

For SI circuits (1) is modified by scaling the voltage vector by 1 Ω to give

$$(s\boldsymbol{C} + s^{-1}\boldsymbol{\Gamma} + \boldsymbol{G})\boldsymbol{I} = \boldsymbol{J}$$

After bilinear transformation and some manipulation, the left matrix decompositions follow exactly as the SC left decompositions and yield the same design equations. These lead to two identical SI low-pass filters with cross-couplings.

The right decompositions for SI implementations are modified to overcome dynamic-range scaling problems and commence with the equations [10]:

$$\boldsymbol{A}\boldsymbol{I} = -\phi[\boldsymbol{B}_l\boldsymbol{W} + \boldsymbol{D}\boldsymbol{I}] + \left[\frac{1+z^{-1}}{1-z^{-1}}\right]\boldsymbol{J}$$

$$\boldsymbol{I}_D\boldsymbol{W} = \psi\boldsymbol{B}_r\boldsymbol{I}$$

Substituting the integrator operators gives

$$\boldsymbol{A}\boldsymbol{I} = -\frac{1}{1-z^{-1}}[\boldsymbol{B}_l\boldsymbol{W} + \boldsymbol{D}\boldsymbol{I}] + \left[\frac{1+z^{-1}}{1-z^{-1}}\right]\boldsymbol{J}$$

$$\boldsymbol{I}_D\boldsymbol{W} = \frac{z^{-1}}{1-z^{-1}}\boldsymbol{B}_r\boldsymbol{I}$$

Applying the frequency shift operator and approximating $\cos\theta \cong 1$ leads to the system equations

$$\boldsymbol{A}\boldsymbol{I} = -\phi[\boldsymbol{B}_l\boldsymbol{W} + \boldsymbol{D}\boldsymbol{I}] + \frac{1+z^{-1}}{1-z^{-1}}\boldsymbol{J} + j\boldsymbol{J}\psi\sin\theta + j\boldsymbol{A}\boldsymbol{I}\psi\sin\theta$$

$$\boldsymbol{I}_D\boldsymbol{W} = \psi\boldsymbol{B}_r\boldsymbol{I} + j\boldsymbol{I}_D\boldsymbol{W}\psi\sin\theta + j\boldsymbol{B}_r\boldsymbol{I}\psi\sin\theta$$

Which again yield two identical cross-coupled low-pass networks.

The same theory applies equally to the design of complex analogue band-stop filters, with the result that two identical high-pass networks with cross-connecting elements are required. It is also possible to derive complex biquad sections for all four techniques. These have been produced and hence cascade realisations for high order complex filters can be utilised.

4 Complex filter designs

The above complex filter design strategies have been implemented in XFILTER [11] and the software has been used to produce a range of designs to illustrate the wide variety of realisations that are viable by various IC techniques.

One of the basic criteria in deciding the feasibility of integrated realisations of analogue circuits is component spread. Table 1 gives typical spread figures for active-RC realisations of complex band-pass elliptic filters of high order; these are all right-LU decompositions. The resistance spread of the 26th order active-RC is well beyond the realistic range for IC implementation.

Tenth order complex elliptic band-pass filters will be used as examples in the following designs. Table 2 summarises the performances of active-RC tenth order complex band-pass and conventional direct band-pass (two normally required in quadrature signal applications) ladder-derived filters. More components are required to realise the direct band-pass circuits, otherwise performance parameters are similar, though the complex case has slightly better noise behaviour. Of course the inherent advantage of the complex

Table 1: Component spreads of active-RC complex elliptic band-pass filters

Order of filter	Capacitance spread	Resistance spread
10	24	131
14	44	252
18	72	409
26	145	906

Table 2: Performance parameters for 10th order active-RC right-LU complex and direct elliptic band-pass filters

	Complex band-pass	Direct band-pass
No. of components	78	116
No. of amps	20	38
C spread	24	10.3
R spread	131	79.5
Max pass-band noise nV/(Hz)$^{1/2}$	58.5	212.2

Table 3: Comparison of complex and direct gm-C 10th order elliptic band-pass filters

	Complex band-pass	Direct band-pass
No. of components	82	118
No. of gm	54	44
C spread	5.9	185.8
gm spread	9.8	1
Max pass-band noise nV/sqrt(Hz)$^{1/2}$	46	268

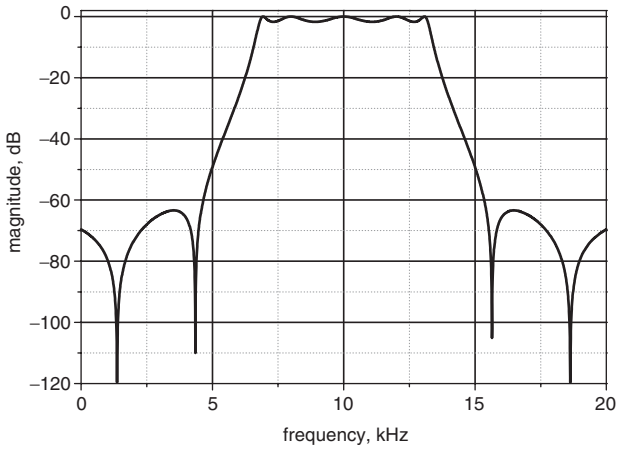

Fig. 2 *Response of 10th-order SC complex band-pass filter*

filter is the ability to reject image frequencies in receiver applications. Table 3 shows a similar pattern for gm-C realisations. However the transconductance spread in the complex case will necessitate many different control loops to define the various gm values, at the cost of extra circuitry.

Figure 2 gives the frequency response of an SC implementation of the complex band-pass filter, using a clock frequency of 660 kHz. The constituent circuits are shown in Figs. 3 and 4. The switches associated with each cross-coupling capacitor may be dispensed with when clocked with the same waveforms as the two low-pass circuits (as in this realisation). They are shown because situations arise when it is necessary to utilise an alternative clocking scheme in order to reduce overall component spread. Figure 5 shows the sum sensitivity of complex and direct SC implementations. A switched-current implementation of the same complex filter shows almost identical sum sensitivity performance. Figure 6 gives typical noise performances of complex and direct SC implementations.

Figure 7 shows a complex band-stop response for a transconductance-C realisation.

Using XFILTER it is possible to examine many alternative circuit solutions and compare relative performance parameters, such as component spreads, sensitivity and noise behaviour.

5 General complex log-domain ladder synthesis

The design of complex log-domain filters offers a rather exciting extension of boundaries in analogue signal processing. The low-voltage, wide-dynamic-range, high-frequency nature of the log-domain approach embedded in the complex filter common to many quadrature receiver architectures should provide an efficient topology for front-end RF receivers. Direct log-domain ladder-filter synthesis is well developed [12] and the complex log-domain filter synthesis method applies a linear transformation to the existing method.

Rewriting (1)

$$\boldsymbol{C}\dot{\boldsymbol{V}} + \boldsymbol{\Gamma}\int \boldsymbol{V} + \boldsymbol{G}\boldsymbol{V} = \boldsymbol{U}V_{IN}$$

where $\boldsymbol{U}$ is a column vector of input connections.

Applying the linear frequency shift ($s \rightarrow s - j\omega_{sh}$) gives

$$\boldsymbol{C}\dot{\boldsymbol{V}} + \boldsymbol{\Gamma}\int \boldsymbol{V} + \boldsymbol{G}\boldsymbol{V} - j\omega_{sh}\boldsymbol{C}\boldsymbol{V} - j\omega_{sh}\boldsymbol{\Gamma}\boldsymbol{V} = \boldsymbol{U}V_{IN} \quad (2)$$

Only the right matrix decomposition yields useful circuits in the log-domain [8], so $\boldsymbol{\Gamma}$ is factorised as

$$\boldsymbol{\Gamma} = \boldsymbol{\Gamma}_L\boldsymbol{\Gamma}_R \quad (3)$$

After introducing an intermediate variable

$$\boldsymbol{X} = \boldsymbol{\Gamma}_R\int \boldsymbol{V} \quad (4)$$

equation (2) can be rewritten as

$$\boldsymbol{C}\dot{\boldsymbol{V}} + \boldsymbol{\Gamma}_L\boldsymbol{X} + \boldsymbol{G}\boldsymbol{V} - j\omega_{sh}\boldsymbol{C}\boldsymbol{V} - j\omega_{sh}\boldsymbol{\Gamma}_L\boldsymbol{\Gamma}_R\boldsymbol{V} = \boldsymbol{U}V_{IN} \quad (5)$$

Equations (4) and (5) describe the linear system, which can be rewritten as

$$\begin{cases} \boldsymbol{C}\dot{\boldsymbol{V}} = \boldsymbol{U}V_{IN} - \boldsymbol{\Gamma}_L\boldsymbol{X} - \boldsymbol{G}\boldsymbol{V} \\ \quad -[-j\omega_{sh}\boldsymbol{C}]\boldsymbol{V} - j\omega_{sh}\boldsymbol{\Gamma}_L\boldsymbol{\Gamma}_R\boldsymbol{V} \\ \boldsymbol{I}_D\dot{\boldsymbol{X}} = \boldsymbol{\Gamma}_R\boldsymbol{V} \end{cases} \quad (6)$$

where $\boldsymbol{I}_D$ is the identity matrix.

The externally linear vectors of $\boldsymbol{V}$ and $\boldsymbol{X}$ can be exponentially mapped to nonlinear internal vectors [13] using

$$Y_i \Rightarrow e^{Y_i/k} = W_{Y_i} \text{ and } \dot{W}_{Y_i} = \frac{1}{k}e^{Y_i/k}\dot{Y}_i \quad (7)$$

where $k = V_T$ for bipolar and $k = nV_T$ for CMOS weak-inversion implementation. Applying (7) to (6) results in a system of equations

$$\begin{cases} \dfrac{C_{ii}}{k}e^{V_i/k}\dot{V}_i = U_i e^{V_{in}/k} - \displaystyle\sum_j \Gamma_{L_{ij}}e^{X_i/k} - G_{ii}e^{V_i/k} \\ \quad -j\omega_{sh}C_{ij}e^{V_i/k} - j\omega_{sh}\Gamma_{L_{ij}}\Gamma_{R_{ij}}e^{V_i/k} \\ \dfrac{I_{D_{ij}}}{k}e^{\frac{X_i}{k}}\dot{X}_i = \displaystyle\sum_j \Gamma_{R_{ij}}e^{V_j/k} \end{cases} \quad (8)$$

Setting $\hat{V}_{in} = e^{V_{in}/k}$ and rewriting in log-domain W variables (8) becomes

$$\begin{cases} C_{ii}\dot{W}_{V_i} = U_i\hat{V}_{in} - \displaystyle\sum_j \Gamma_{L_{ij}}W_{X_j} - G_{ii}W_{V_i} \\ \quad -j\omega_{sh}C_{ij}W_{V_i} - j\omega_{sh}\Gamma_{L_{ij}}\Gamma_{R_{ij}}G_{ii}W_{V_i} \\ I_{D_{ij}}\dot{W}_{X_i} = \displaystyle\sum_j \Gamma_{R_{ij}}W_{V_j} \end{cases} \quad (9)$$

After 'real' and 'imaginary' part extraction, (9) becomes

$$\begin{cases} C_{ii}\dot{W}^{\mathrm{Re}}_{V_i} = U_i\hat{V}^{\mathrm{Re}}_{in} - \displaystyle\sum_j \Gamma_{L_{ij}}W^{\mathrm{Re}}_{X_j} - G_{ii}W^{\mathrm{Re}}_{V_i} \\ \quad +\omega_{sh}C_{ij}W^{\mathrm{Im}}_{V_i} + \omega_{sh}\Gamma_{L_{ij}}\Gamma_{R_{ij}}G_{ii}W^{\mathrm{Im}}_{V_i} \\ I_{D_{ij}}\dot{W}^{\mathrm{Re}}_{X_i} = \displaystyle\sum_j \Gamma_{R_{ij}}W^{\mathrm{Re}}_{V_j} \\ C_{ii}\dot{W}^{\mathrm{Im}}_{V_i} = U_i\hat{V}^{\mathrm{Im}}_{in} - \displaystyle\sum_j \Gamma_{L_{ij}}W^{\mathrm{Im}}_{X_j} - G_{ii}W^{\mathrm{Im}}_{V_i} \\ \quad -\omega_{sh}C_{ij}W^{\mathrm{Re}}_{V_i} - \omega_{sh}\Gamma_{L_{ij}}\Gamma_{R_{ij}}G_{ii}W^{\mathrm{Re}}_{V_i} \\ I_{D_{ij}}\dot{W}^{\mathrm{Im}}_{X_i} = \displaystyle\sum_j \Gamma_{R_{ij}}W^{\mathrm{Im}}_{V_j} \end{cases} \quad (10)$$

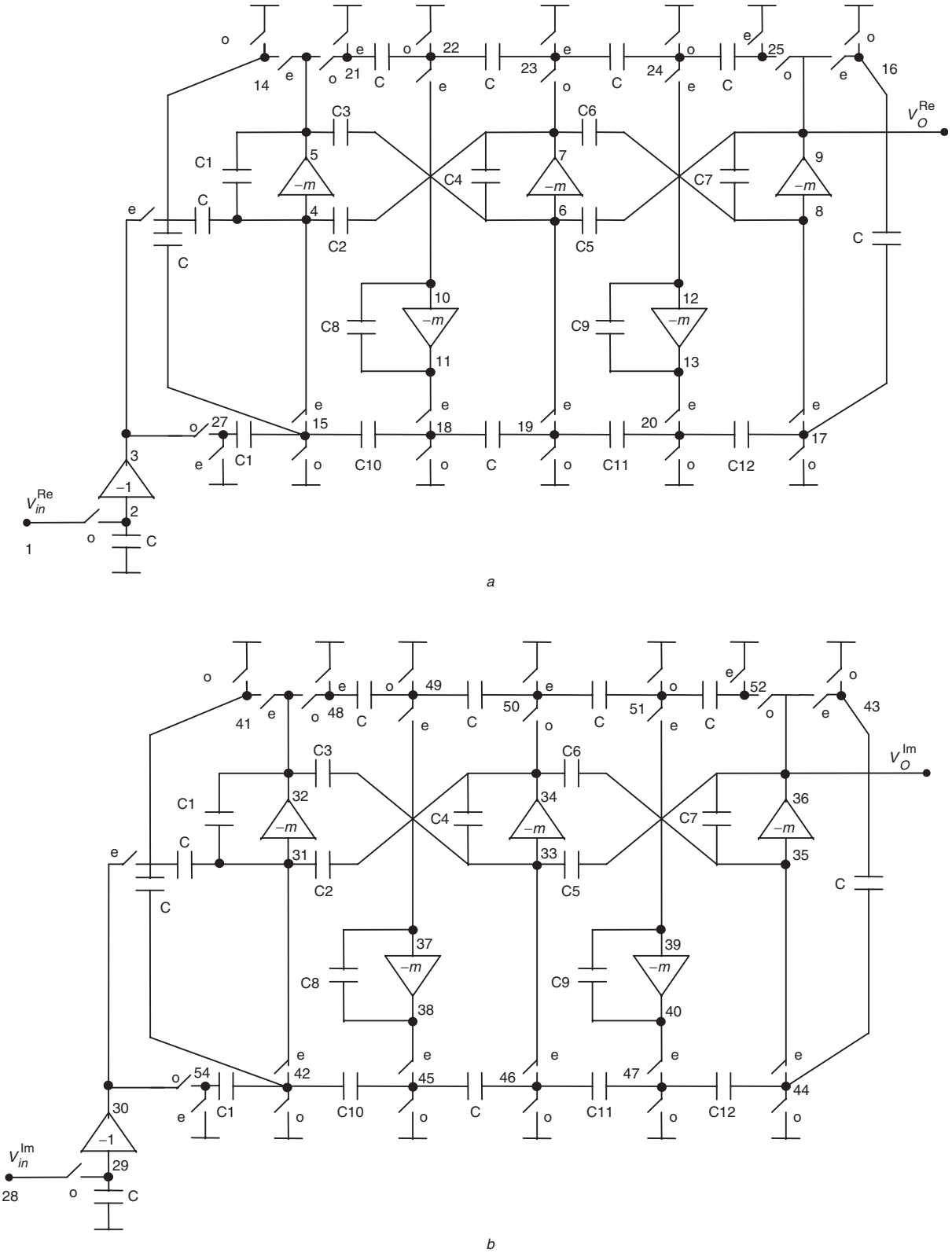

Fig. 3 *Low-pass right-LU circuit (real and imaginary) for 10th order complex SC band-pass filter*
a Real
b Imaginary

The system (10) presents a general form of a complex log-domain ladder filter. This can be easily extended [12] to include zero-producing sections and, hence, more general log-domain ladder-derived filters. These equations represent two identical low-pass filters with cross-coupling to produce a log-domain complex band-pass filter or two identical high-pass filters with cross-coupling to produce an equivalent band-stop filter.

5.1 First-order complex log-domain integrator block

An integrator is a necessary building block and in the frequency domain the transfer function of a first-order complex coefficient system can be expressed as [6]

$$H(s) = \frac{Y}{X} = \frac{A}{1 + Bs - j\omega_{sh}} \tag{11}$$

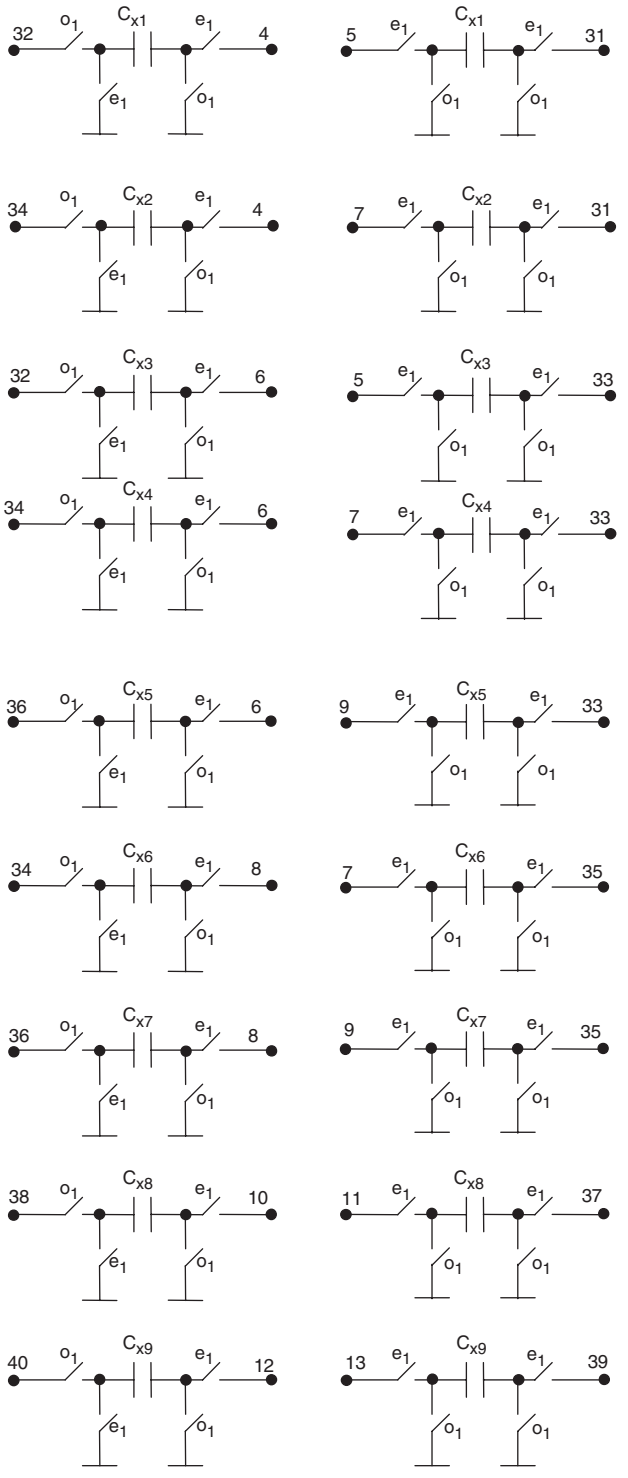

Fig. 4 *Cross-couplings for 10th-order complex SC band-pass filter* $C_{xn} = C_n \sin\theta$

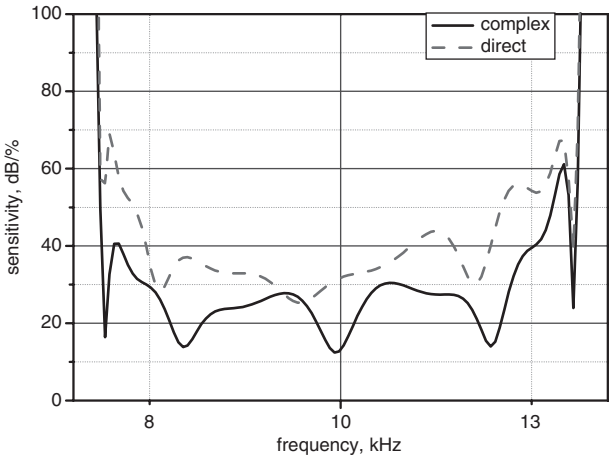

Fig. 5 *Sum-sensitivities of SC 10th-order elliptic band-pass circuits*

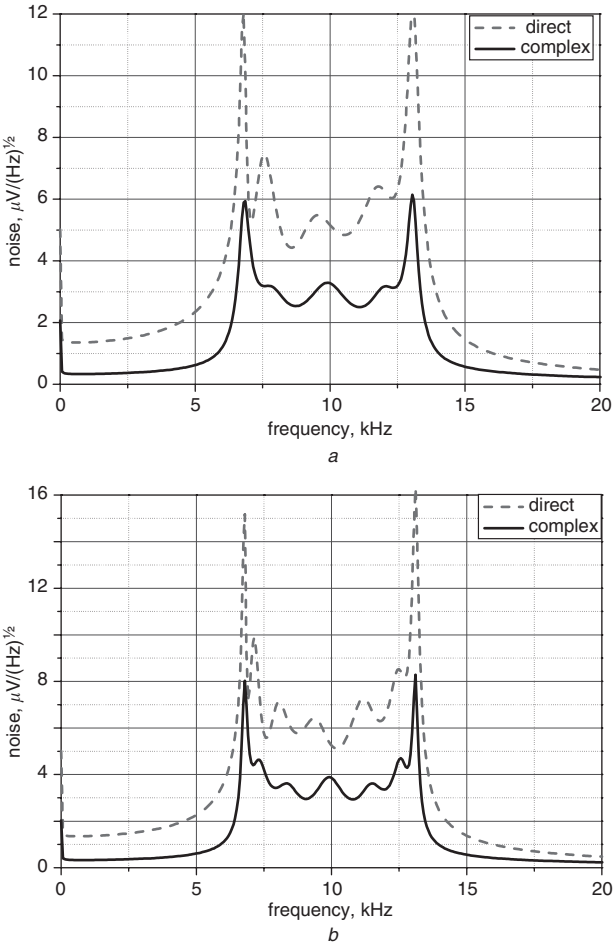

Fig. 6 *Noise performance of 10th- and 14th-order SC complex and direct band-pass circuits*
a 10th-order
b 14th-order

In the time domain this becomes

$$B\dot{Y} + Y - j\omega_{sh}Y = AX \tag{12}$$

Nonlinear mapping of (12) leads to

$$\frac{B}{k}\dot{Y}e^{Y/k} + e^{Y/k} - j\omega_{sh}e^{Y/k} = Ae^{Y/k} \tag{13}$$

or in log-domain W variables

$$B\dot{W}_Y + W_Y - j\omega_{sh}W_Y = A\hat{X} \tag{14}$$

The 'real' part of the system is

$$B\dot{W}_Y^{\mathrm{Re}} = A\hat{X}^{\mathrm{Re}} - W_Y^{\mathrm{Re}} + \omega_{sh}W_Y^{\mathrm{Im}} \tag{15}$$

The 'imaginary' part of the system is

$$B\dot{W}_Y^{\mathrm{Im}} = A\hat{X}^{\mathrm{Im}} - W_Y^{\mathrm{Im}} + \omega_{sh}W_Y^{\mathrm{Re}} \tag{16}$$

and this can be shown diagrammatically, Fig. 8, which indicates two identical subsystems with cross connections between the integrator blocks. Comparison of (15) and (16) with (10) shows a similar structure and these complex log-domain integrators can be used in the realisation of general complex log-domain filters. A variety of complex integrator types can be utilised in synthesis. One design based on a well

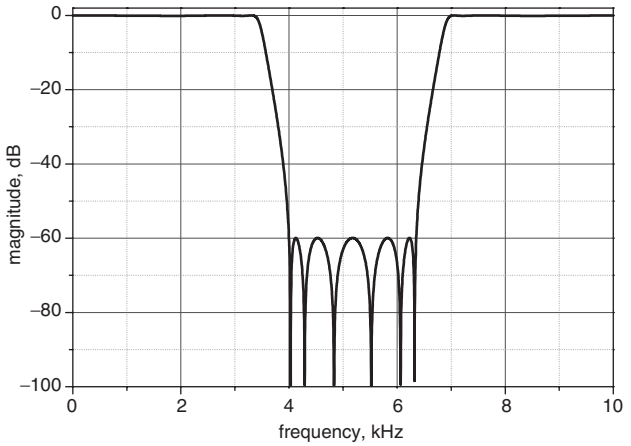

Fig. 7 *Frequency response of 12th-order gm-C biquad complex band-stop filter*

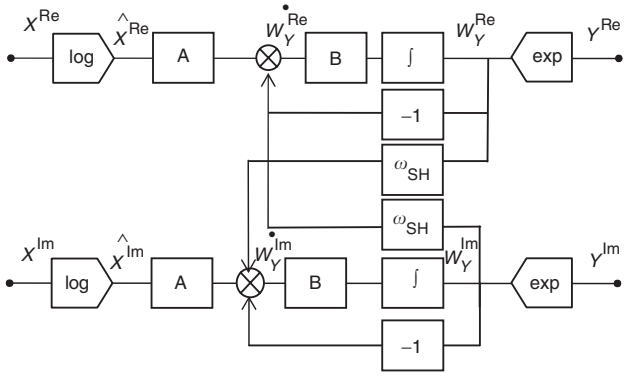

Fig. 8 *First-order log-domain complex system*

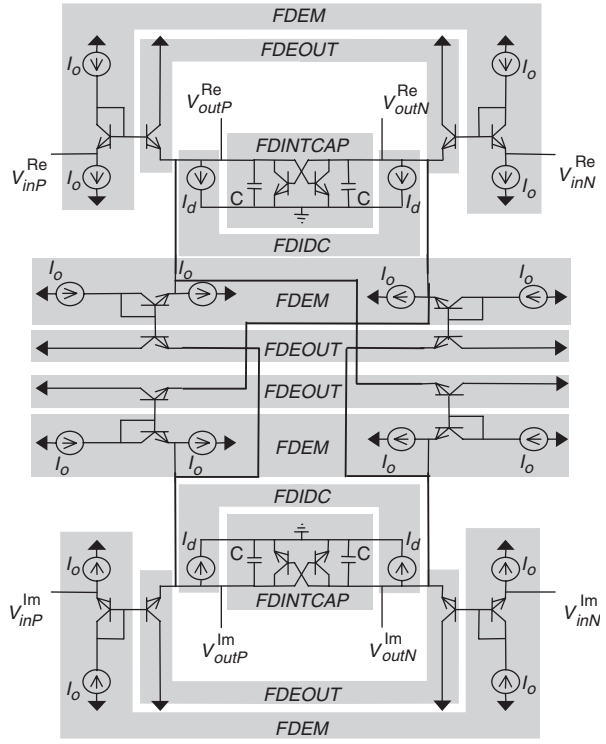

Fig. 9 *Complex log-domain integrator*

known fully differential integrator [12] is shown in Fig. 9. This fully differential structure is incorporated into XFILTER software to provide fully differential in-phase and quadrature signals throughout.

6 Complex log-domain cascade-biquadratic filters

The alternative approach to realising a transfer function of any order is by cascading second- and first-(if odd order) order blocks. A complex log-domain biquadratic section is shown in Fig. 10 and a first-order complex log-domain section is given in Fig. 11. These are derived from standard log-domain sections [9]. The value of cross-connection current is expressed as $I_{\omega sh} = \omega_{sh} C V_T$ where C is capacitor value, V_T is thermal voltage and ω_{sf} is shifting frequency.

7 Complex group-delay equalisers

Applying the frequency-shift technique to the ladder-derived all-pass method [14] again leads to cross-coupled structures in all the realisation techniques discussed. A log-domain version is shown in Fig. 12. $Y(s)$ is a singly terminated ladder which can be synthesised by the log-domain technique. Cross-coupled all-pass biquadratic

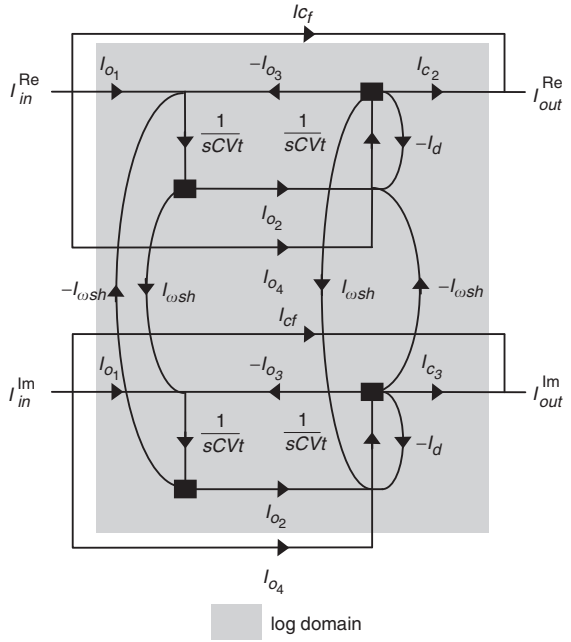

Fig. 10 *Complex log-domain biquadratic section*

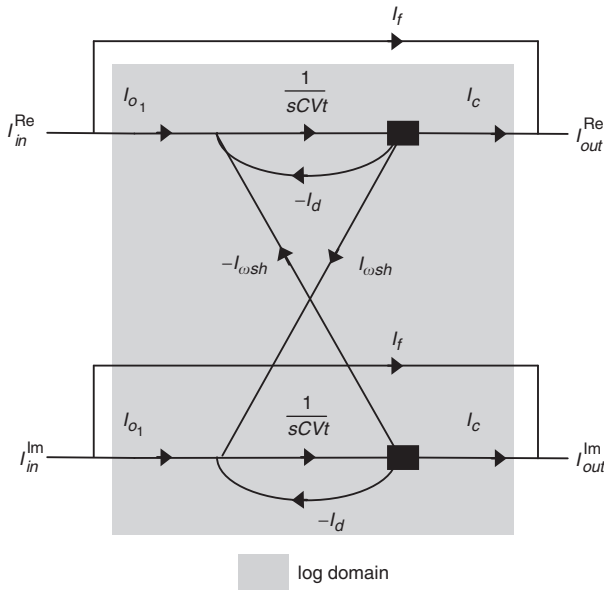

Fig. 11 *First-order complex log-domain section*

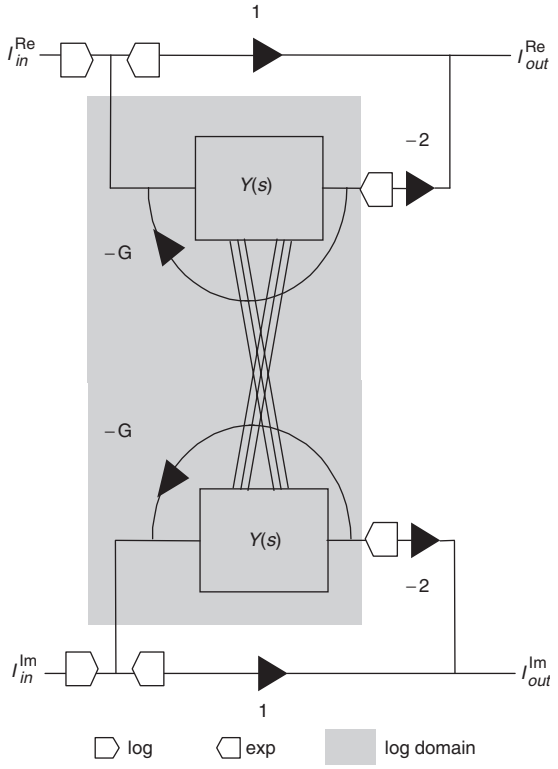

Fig. 12 *Complex log-domain ladder all-pass equaliser*

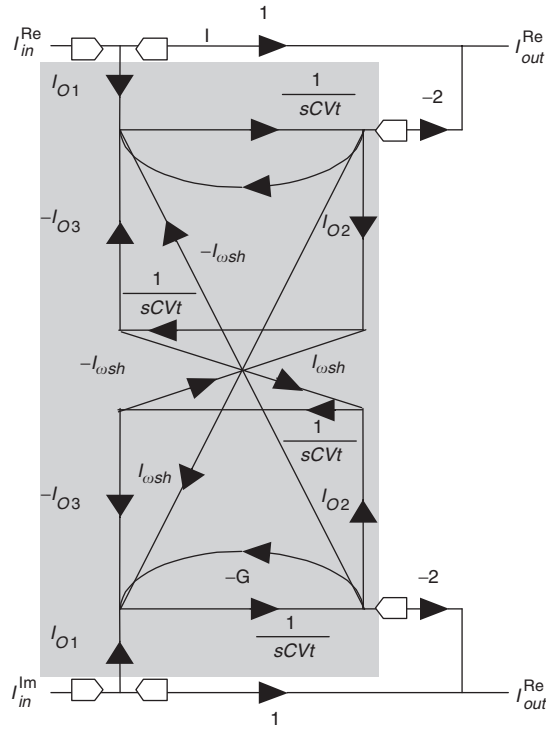

Fig. 13 *Complex log-domain all-pass biquad*

sections can similarly be derived and typical log-domain versions are shown in Figs. 13 and 14.

8 Log-domain design example

The synthesis procedures for both ladder and biquad complex log-domain filters and equalisers have been implemented in XFILTER. The frequency responses of a typical tenth order 0.5 dB ripple Chebyshev band-pass filter

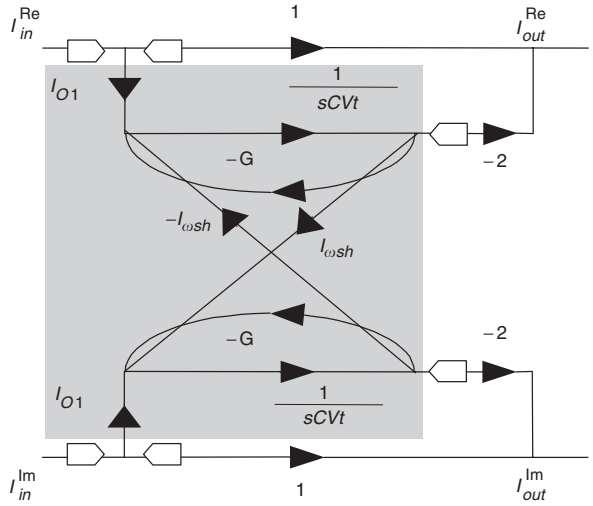

Fig. 14 *Complex log-domain all-pass first-order section*

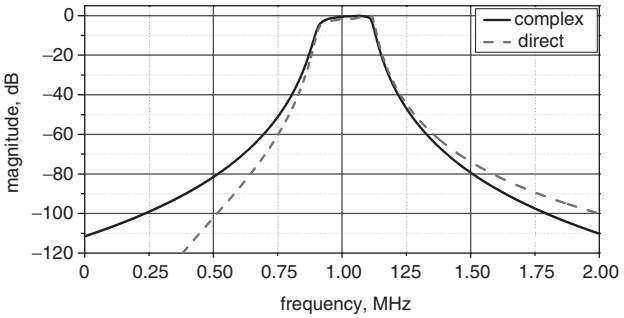

Fig. 15 *Tenth-order Chebyshev filter frequency responses*

Table 4: Comparison of complex and direct log-domain 10th order Chebyshev band-pass filters

	Complex band-pass	Direct band-pass
No. of Transistors	440	840
No. of Capacitors	20	40
C spread	2.02	1.3
Total *I*	379.9 μA	1.642 μA
I spread	36.9	12.1
Max pass-band noise pA/sqrt(Hz)$^{1/2}$	83	70

for log-domain direct and complex realisations are shown in Fig. 15. These were computed by Spectre using real transistor models (typical BSim3v3 model for a targeted 0.6 μm complementary bipolar process). They illustrate the inherent difference between direct and complex realisations, due to the application of a low-pass/band-pass transformation in the former and the linear frequency shift in the latter. Table 4 shows typical circuit parameters, and the overall low noise performance of log-domain realisations is noticeable. The noise responses in Fig. 16 were computed with SpectreRF. The noise performance for the complex realisation is higher, possibly due to the larger number of transistors in each signal path. This behaviour varies with filter type. The group delay responses in Fig. 17 show the effective equalisation of group delay on the complex filter using two identical cross-coupled sixth-order log-domain all-pass equaliser networks.

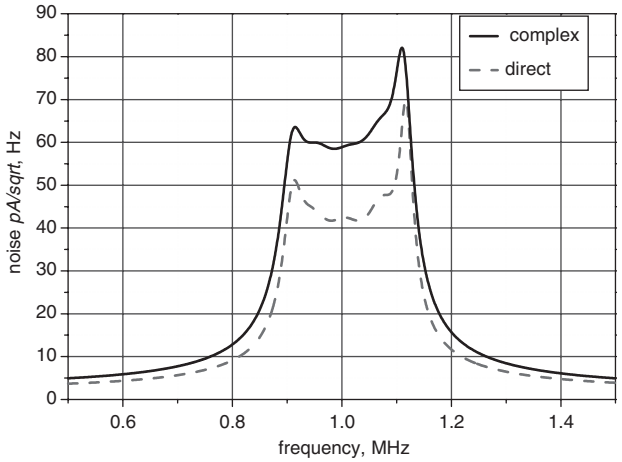

Fig. 16 *Tenth-order Chebyshev filter noise responses*

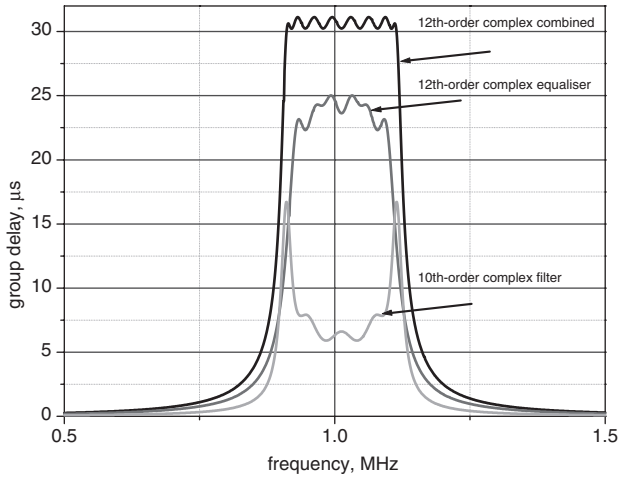

Fig. 17 *Simulated complex group-delay responses*

9 Conclusions

Methods for the synthesis of complex analogue filters as both ladder and cascade-biquad realisations have been described. These general routines have been implemented in the XFILTER software. They have been used to design a variety of complex band-pass and band-stop filters. Typical examples are shown and performance results are presented. The spread in component values of complex filter realisations of all types is dominated by values of the cross-coupling elements, and the spread in the low-pass or high-pass constituent filters is usually well conditioned. Many solutions can be examined in the design process and an optimum realisation can be selected. In particular, complex log-domain filters have many interesting properties and further work is continuing to evaluate these and improve practical designs.

10 Acknowledgments

Financial support from the Engineering and Physical Sciences Research Council (GR/M 45252) is gratefully acknowledged.

11 References

1 Snelgrove, W.M., and Sedra, A.S.: 'State-space synthesis of complex analog filters'. Proc. European Conf. on Circuit Theory and Design, ECCTD, The Hague, The Netherlands, 1981, pp. 420–424
2 Lui, Q., Snelgrove, W.M., and Sedra, A.S.: 'Switched-capacitor implementation of complex filters'. Proc IEEE Int. Symp. on Circuits and Systems, ISCAS, San Jose, CA, USA, May 1986, pp. 1121–1123
3 Muto, C., and Kambayashi, N.: 'A leapfrog synthesis of complex analog filters', *IEICE Trans.*, 1993, **E76-A**, (2), pp. 210–215
4 Muto, C., and Kambayashi, N.: 'A realisation of real filters using complex resonators', *Electron. Commun. Jpn., 3, Random Electron. Sci.*, 1993, **36**, (3)
5 Zhang, X., Iwahashi, M., and Kambayashi, N.: 'A novel narrow-band band-pass filter and its application to SSB communication', *IEICE Trans.*, 1997, **E80-C**, (7), pp. 1010–1015
6 Crols, J., and Steyaert, M.S.J.: 'Low-IF topologies for high-performance analog front ends of fully integrated receivers', *IEEE Trans. Circuits Syst. II, Analog Digit. Signal Process.*, 1998, **45**, (3), pp. 269–282
7 Minnis, B.J., Moore, P.A., Payne, A.W., Davie, A.J., and Greer, N.P.J.: 'A low-IF, polyphase receiver for DECT'. Proc. IEEE Int. Symp. on Circuits and Systems ISCAS, Geneva, Switzerland, May 2000, pp. 83–86
8 Ping, L., Henderson, R.K., and Sewell, J.I.: 'A methodology for integrated ladder filter design', *IEEE Trans. Circuits Syst.*, 1991, **38**, (8), pp. 853–868
9 Greer, N.P.J., Henderson, R.K., Ping, L., and Sewell, J.I.: 'Matrix methods for the design of transconductor ladder filters', *IEE Proc., Circuits Devices Syst.*, 1994, **141**, (2), pp. 89–100
10 Ng, A.E.J., and Sewell, J.I.: 'Feasible designs for high order switched-current filters', *IEE Proc., Circuits Devices Syst.*, 1998, **146**, (5), pp. 297–305
11 Teplechuk, M.A. and Sewell, J.I. 'XFILT reference manual v.4.0', Univ. of Glasgow, Dept of Electronics and Elect. Eng., UK, 2004
12 Ng, A.E.J., Sewell, J.I., Drakakis, E.M., Payne, A.J., and Toumazou, C.: 'A unified matrix method for systematic synthesis of log-domain ladder filters'. Proc. IEEE Int. Symp. on Circuits and Systems, ISCAS 2001, Sydney, Australia, 2001, Vol. 1, pp. 149–152
13 Frey, D.R.: 'Log-domain filtering: an approach to current-mode filtering', *IEE Proc. G, Circuits Devices Syst.*, 1993, **140**, pp. 406–416
14 Ng, A.E.J., and Sewell, J.I.: 'Log-domain allpass group-delay equaliser design with XFILTER'. Proc. IEEE Int. Conf. on Electronics, Circuits and Systems, ICECS, Dubrovnik, Croatia, Sept. 2002, Vol. 1, pp. 125–128